

On the evolutions of triple point structure in wedge-stabilized oblique detonations

Cite as: Phys. Fluids 34, 067118 (2022); doi: 10.1063/5.0090975

Submitted: 10 March 2022 · Accepted: 2 June 2022 ·

Published Online: 17 June 2022



View Online



Export Citation



CrossMark

Zhenye Luan (栾振业),¹ Yue Huang (黄玥),^{1,a)} Ralf Deiterding,² and Yancheng You (尤延铖)¹

AFFILIATIONS

¹School of Aerospace Engineering, Xiamen University, Xiamen 361005, China

²School of Engineering, University of Southampton, Southampton SO16 7QF, United Kingdom

^{a)}Author to whom correspondence should be addressed: huangyue@xmu.edu.cn

ABSTRACT

The oblique detonation induced by a two-dimensional semi-infinite wedge is simulated numerically with the Navier–Stokes equations and a detailed H₂/air reaction model based on the open-source program-Adaptive Mesh Refinement in Object-oriented C++. A spatially seventh-order-accurate essentially non-oscillatory scheme is adopted for the convective flux discretization. The formation and evolution of the oblique detonation induced by wedges at different angles and inflow conditions are investigated, and a prediction model for the oblique detonation flow field is proposed. The results show that the formation of the oblique detonation flow field can be divided into two processes. The first process is similar to the oblique shock flow field with unreactive inflow. When the inflow passes through the wedge, the oblique shock wave starts to form at the tip, followed by the unstable curved shock surface and triple point. In this process, a thin reaction layer is formed on the wedge front, but the thickness of the reaction layer is almost constant. The second process is similar to the process of deflagration to detonation. As the reaction rate increases, the deflagration front is fixed on the wedge, the reaction layer thickens, and the deflagration front gradually approaches the oblique shock wave. When the deflagration front is coupled with the oblique shock wave, the oblique detonation is formed. Moreover, a theoretical prediction model for the triple point location is proposed. Compared with the numerical simulation results, the theoretical model prediction for the position of the transition point of the oblique shock wave–oblique detonation wave is relatively acceptable.

Published under an exclusive license by AIP Publishing. <https://doi.org/10.1063/5.0090975>

I. INTRODUCTION

An oblique detonation engine (ODE) is a potential propulsion device based on a stationary oblique detonation wave (ODW). The oblique detonation in the combustion chamber is induced by supersonic reactive inflow over a wedge, which is relevant and close to practical configurations for hypersonic propulsion operation. It has received much attention since the 1980s due to its potential advantages of greater efficiency and shorter combustor length in comparison with the traditional scramjet. However, the formation and the stabilization mechanism of an ODW have not been clearly explained theoretically.^{1–6}

A wealth of analytic and numerical studies on the fundamental issues about the ODW induced by the wedge can be found in the literatures. The early theoretical solutions of oblique detonations under different shock angles and the ODW structures as the basic foundation were obtained by the pioneering works of Gross,¹ Pratt *et al.*,² Powers *et al.*,^{3,7,8} and Emanuel *et al.*⁹ using the reactive Rankine–Hugoniot analysis, in which the ODW is approximated as an oblique shock

wave (OSW) coupled with an instantaneous heat release from the reaction zone. The method of characteristics with a one-step Arrhenius chemistry model was developed by Verreault *et al.*¹⁰ to simulate ODW initiation from a wedge. This resulted in the determination of the wave-angle evolution. A simplified characteristics formulation of linearized Euler equations and linearized Rankine–Hugoniot jump conditions across the leading oblique shock were employed more recently by Martínez-Ruiz *et al.*^{11,12} to analyze the OSW–ODW transition in wedge-induced oblique detonations. The characteristics of wedge-induced OSW–ODW transitions are mainly affected by reaction kinetics. A one-step Arrhenius chemistry model with sufficiently large activation energies can lead to a transition occurring at a triple point for a wide range of combinations of incoming Mach number and wedge angle. Since the detailed flow structure of an oblique detonation under different OSW–ODW transition types is difficult to describe by experimental measurement, high-precision numerical simulation has become the main research method for oblique detonation under high Mach number conditions.

The basic formation structures of an ODW attached to a wedge were first addressed in the pioneering simulation work of Li *et al.*¹³ The OSW–ODW transition occurs abruptly at a triple point, which is usually referred to as the abrupt transition mode. The smooth transition mode of the OSW–ODW was first shown in the numerical simulations of Vlasenko *et al.*¹⁴ and was confirmed in the numerical study by Da Silva *et al.*¹⁵ Two distinct OSW–ODW transition modes have been verified numerically for a wide range of chemical kinetics, free-stream Mach numbers, and wedge angles. Ghorbanian and Sterling¹⁶ have numerically analyzed the formation of oblique detonation over a variable-polar-ramp and shown reaction-polar diagrams, suggesting that the formation process of oblique detonation is analogous to deflagration to detonation (DDT). Sislian *et al.*¹⁷ described the effects of incomplete fuel/air mixing on two types of ramjets performance characteristics by assuming a Gaussian distribution of equivalence ratio in the combustible mixture flow, and the deflagration distortion is observed clearly. The formation and stability of a near-CJ ODW were numerically investigated by Fusina *et al.*¹⁸ It was found that the ODW is shown to be resilient to inhomogeneities in the oncoming fuel-air mixture, and the induction process and radical formation within the ODW structure were analyzed. Zhang *et al.*¹⁹ studied the formation of ODW with various equivalence ratios and found that the initiation length as a function of equivalence ratio displays a classical “V-shaped” curve, similar to the relation between detonation cell size and initiation energy.²⁰ Teng *et al.* solved the Euler equation with a two-step chemical model to investigate the factors influencing the flow structure of ODW²¹ and the effect of periodic inflow on ODW instabilities.²² Zhang *et al.* solved the Euler equation with a single-step chemical model to investigate the evolution of ODW structure and the effects of activation energy on ODW instabilities.²³ Iwata *et al.*²⁴ simulated the shock-induced combustion from a supersonic spherical projectile, illustrating several shock-flame configurations induced by inflow equivalence ratio inhomogeneity. They also performed simulations on wedge-stabilized oblique detonations²⁵ with different Gaussian equivalence ratio distributions, demonstrating that the near-wedge deflagration fronts are distorted into a complicated surface, generating the so-called “V-shaped” deflagration front and “V + Y” Mach stem. Fang *et al.*²⁶ focused on the formation and characteristic parameters of the oblique detonation wave with inhomogeneous mixing of hydrogen and air inflow for a better understanding of oblique detonation wave engine performance under practical operating conditions. Bachman and Goodwin²⁷ presented a new ignition criterion curve that was added to the traditional stability limits in order to include the effects of chemical kinetic timescales and wedge surface length on the prediction of ignition and formation of ODWs. This ignition criterion was demonstrated to accurately predict the formation and ignition location of an ODW on an inviscid wedge surface. Since two-dimensional numerical simulations are computationally demanding, numerical studies tend to focus on a limited number of cases (e.g., by fixing the wedge angle or the incoming stream's properties) so that only limited portions of the accessible parametric space are explored. As a result, despite significant work, there is still a lack of a complete parameter specification for ODW formation, which makes it impossible to predict the structure and the transition type of ODW.

This paper analyzes the change of the relative position of flame and OSW in the process of the initiation of the ODW flow field. The influence of different wedge angles on the flow field in the engine in a

real situation is simulated in the hope of summarizing some rules for the prediction of oblique detonation structure. The paper is organized as follows. Section II summarizes the numerical methods used to solve the equations and the calculation model for the simulations. In Sec. III, the AMROC code and the convergence of grid resolution are verified. Section IV analyzes the results and discusses the formation of the ODW flow field and the gradual combustion enhancement process during the formation of ODW. Section V contains our conclusions.

II. NUMERICAL METHOD AND CALCULATION MODEL

A. Numerical method

The system of governing equations is the two-dimensional compressible reactive Navier–Stokes equations, which we write in the form of an inhomogeneous convection–diffusion equation as

$$\frac{\partial Q}{\partial t} + \frac{\partial(F_x - G_x)}{\partial x} + \frac{\partial(F_y - G_y)}{\partial y} = S. \quad (1)$$

In Eq. (1), Q is the vector of state quantities, F_x and F_y are the convective fluxes, and S is the chemical reaction source term, which are defined as

$$Q = \begin{bmatrix} \rho_i \\ \rho u \\ \rho v \\ \rho E \end{bmatrix}, \quad F_x = \begin{bmatrix} \rho_i u \\ \rho u^2 + p \\ \rho u v \\ u(\rho E + p) \end{bmatrix}, \quad (2)$$

$$F_y = \begin{bmatrix} \rho_i v \\ \rho u v \\ \rho v^2 + p \\ v(\rho E + p) \end{bmatrix}, \quad S = \begin{bmatrix} \dot{\omega}_i \\ 0 \\ 0 \\ 0 \end{bmatrix},$$

where $i = 1, 2, \dots, N_{sp}$ and N_{sp} is the number of species. In Eq. (1), G_x and G_y are the fluxes of the diffusion terms, which are defined as

$$G_x = \begin{bmatrix} \rho D_i (\partial Y_i / \partial x) \\ \tau_{xx} \\ \tau_{xy} \\ k(\partial T / \partial x) + \rho \sum_{j=1}^{N_{sp}} h_j D_j (\partial Y_j / \partial x) + u \tau_{xx} + v \tau_{xy} \end{bmatrix}, \quad (3)$$

$$G_y = \begin{bmatrix} \rho D_i (\partial Y_i / \partial y) \\ \tau_{yx} \\ \tau_{yy} \\ k(\partial T / \partial y) + \rho \sum_{j=1}^{N_{sp}} h_j D_j (\partial Y_j / \partial y) + u \tau_{xy} + v \tau_{yy} \end{bmatrix}. \quad (4)$$

In Eqs. (3) and (4), Y_i is the mass fraction of component i in the mixed gas, which can be obtained by the ratio of the partial densities with respect to the total density of the mixture, $Y_i = \frac{\rho_i}{\rho} D_i$ and D_i represent the mixture diffusion coefficients, $k(\partial T / \partial x)$ and $k(\partial T / \partial y)$ represent the energy fluxes caused by heat conduction, $\rho \sum_{j=1}^{N_{sp}} h_j D_j (\partial Y_j / \partial x)$

and $\rho \sum_{j=1}^{N_p} h_j D_j (\partial Y_j / \partial y)$ represent the energy fluxes caused by species diffusion, and τ is the viscous stress tensor, which is specified as

$$\begin{aligned}\tau_{xx} &= -(2/3)\mu(\nabla \cdot \mathbf{v}) + 2\mu(\partial u / \partial x), \\ \tau_{yy} &= -(2/3)\mu(\nabla \cdot \mathbf{v}) + 2\mu(\partial v / \partial y),\end{aligned}\quad (5)$$

$$\tau_{xy} = \tau_{yx} = \mu(\partial u / \partial y + \partial v / \partial x), \quad \text{with } \nabla \cdot \mathbf{v} = (\partial u / \partial x + \partial v / \partial y).\quad (6)$$

In addition, E in Eq. (1) is the total energy per unit mass, which reads

$$E = \sum_{i=1}^{N_{sp}} Y_i h_i - p/\rho + \frac{1}{2}(u^2 + v^2).\quad (7)$$

The quantity h_i is the specific enthalpy of component i , which reads for a thermally perfect gas

$$h_i = h_{ref}^0 + \int_{T_{ref}}^T c_p dT.\quad (8)$$

The variable $\dot{\omega}_i$ is the mass generation rate of component i , which can be obtained by a detailed chemical reaction mechanism consisting of J reactions as

$$\begin{aligned}\dot{\omega}_i &= \sum_{j=1}^J \left(\nu_{ji}^r - \nu_{ji}^f \right) \left[k_j^f \prod_{n=1}^{N_{sp}} (\rho_n / W_n)^{\nu_{jn}^f} - k_j^r \prod_{n=1}^{N_{sp}} (\rho_n / W_n)^{\nu_{jn}^r} \right], \\ i &= 1, \dots, N_{sp},\end{aligned}\quad (9)$$

where ν_{ji}^f and ν_{ji}^r represent stoichiometric coefficients of forward and reverse chemical reaction. W_n represents the molar mass of component i . The forward and reverse chemical reaction rate constants are given by Arrhenius's formulas

$$k_j^{f/r}(T) = A_j^{f/r} T^{f/r} \exp \left(-E_j^{f/r} / RT \right).\quad (10)$$

In Eq. (10), activation energy and pre-exponential factor refer to the corresponding chemical reaction mechanism. The ideal gas equation for mixtures is used to close the system of Eq. (1).

The numerical simulations have been carried out using the open-source code AMROC^{28,29} based on a structured adaptive mesh refinement (SAMR) framework.³⁰ An operator splitting technique (or, the method of fractional steps) for the computation of the time-dependent reactive flow (see Ref. 31) is used to solve Eq. (1). This technique allows a decoupled treatment for the time-implicit discretization of the local source term and the time-explicit discretization of the hydrodynamic transport term. The convection terms in Eq. (1) are discretized with the seventh-order WENO-symmetric-order-optimized (WENO-SYMOO) scheme as shown by Martin *et al.*³² The optimal third-order strong stability preserving (SSP) Runge–Kutta scheme³³ is used for time integration in combination with time-splitting and the fourth-order accurate semi-implicit GRK4A method³⁴ for source term integration. A detailed H₂–Air reaction mechanism including 9 species (O₂, H₂O, H, O, OH, H₂, HO₂, H₂O₂, and N₂) and 34 elementary reactions has been used.³⁵

B. Calculation model

Figure 1 shows the two-dimensional computational domain and boundary conditions. The two-dimensional rectangular region is

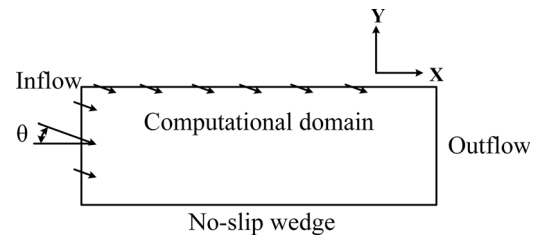


FIG. 1. Schematic of the computational domain and boundary conditions.

selected to make the boundary and structured grid parallel to the Cartesian coordinate axis (X-axis and Y-axis), respectively, so as to eliminate the calculation error caused by the, otherwise, non-Cartesian oblique boundary. The left boundary and upper boundary are free to stream boundary conditions. The right boundary is opened to the atmosphere with the outflow boundary condition. The lower boundary represents the wedge surface that is set as no-slip boundary condition. The angle between the free stream and the X-axis is θ .

The initial conditions of the cases calculated in the paper are shown in Table I. The free stream is a mixture of hydrogen, oxygen, and nitrogen with a mole fraction ratio of 2:1:3.76. The difference in oblique detonation flow field is compared when the wedge angle θ is 15° (case 1), 20° (case 2), and 25° (case 3). Considering a flight altitude of 30 km and a flight Mach number of 10, the ambient flow is pre-compressed twice by weak oblique shock waves in the aircraft inlet. The deflection angle is 12.5°. Therefore, the inflow temperature of 1021 K, the inflow pressure of 56 kPa, and inflow Mach number of 4.3 are obtained.³⁶ The computational domains along the X- and Y- axis are (-1 mm, 79 mm) and (0, 20 mm), respectively. The position of the vertex of the wedge in the computational domain is (0 mm, 0 mm). The computational base cell size is set to 25 × 25 μm^2 and refined to up to 3.125 × 3.125 μm^2 adaptively on-the-fly. The half-reaction length (hrl) is 0.59314 mm for the current initial conditions, as calculated by Cantera,³⁷ which corresponds to about 190 points per half-reaction length (190 pts/hrl).

III. VERIFICATION OF CODE AND GRID RESOLUTION

To verify the accuracy of the numerical simulation, the model and grid resolution are validated. First of all, based on the work by Viguerie,³⁸ the comparison of numerical and experimental ODW field with the results calculated by the code in this paper are displayed in Fig. 2 with the same inflow conditions. The experiment is performed by a positive detonation that generates a high Mach number gas flow and drives the Mylar film (gaseous wedge) to the left with a constant speed and angle into the hydrogen–air section. As can be seen in Fig. 2(a), the numerical

TABLE I. Initial conditions of the cases calculated in the paper.

	T (K)	P (kPa)	Ma	Wedge angle θ (°)	Mole fraction (H ₂ :O ₂ :N ₂)
Case 1	1021	56	4.3	15	2:1:3.76
Case 2	1021	56	4.3	20	2:1:3.76
Case 3	1021	56	4.3	25	2:1:3.76
Case 4	765	33.5	3.94	20	2:1:3.76

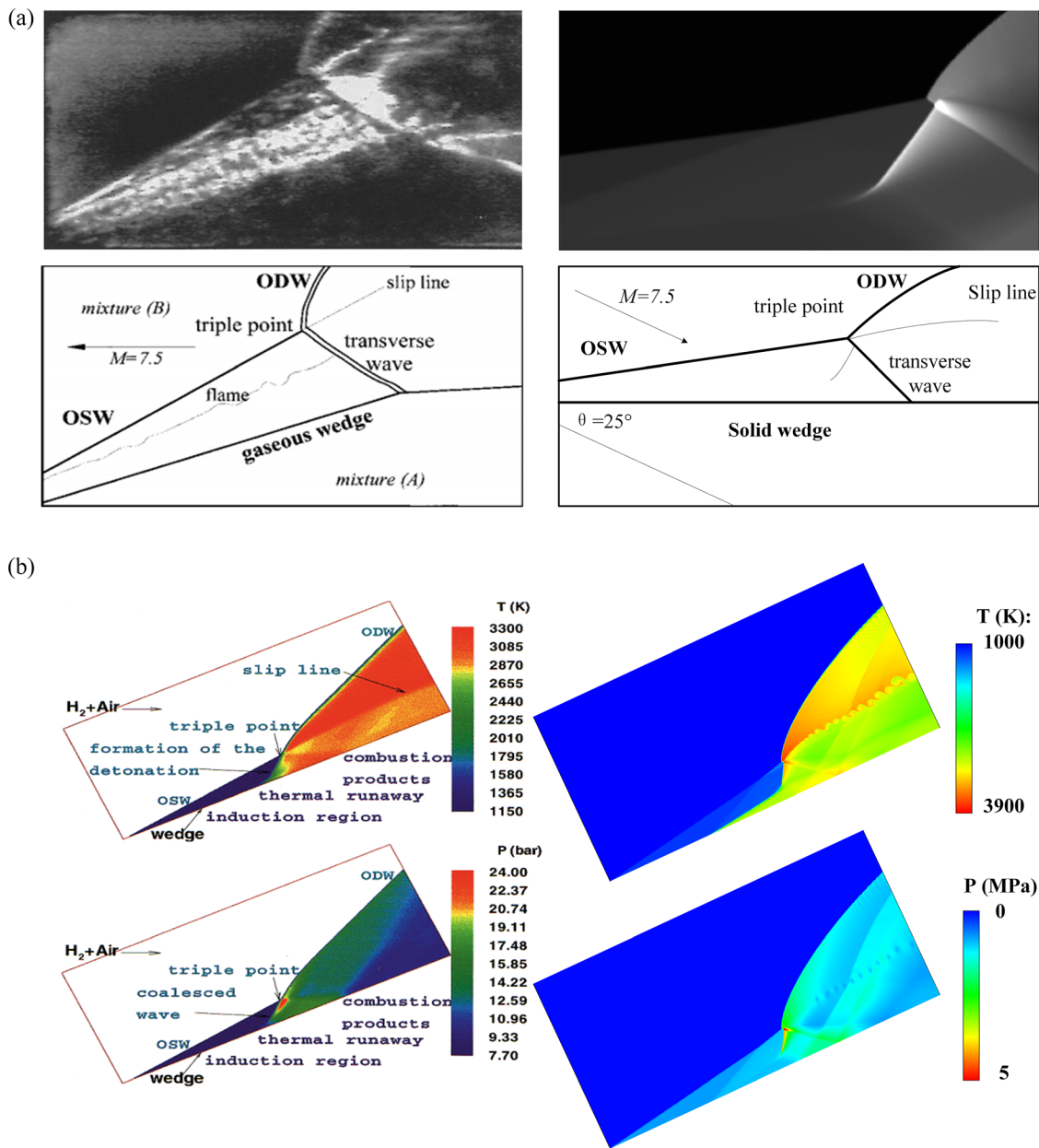


FIG. 2. Comparison of (a) experimental and (b) numerical results between Viguier³⁸ and simulation using AMROC.

schlieren of the ODW field calculated by AMROC agrees well with the experimental ODW field. Typical structures and phenomena can be clearly distinguished: OSW, triple point, ODW, slip line, and transverse wave. Similarly, the comparison of numerical simulation results is also highly consistent, as shown in Fig. 2(b). Moreover, the detonation angle obtained from the experimental and numerical results using AMROC is 49° and 47° , respectively, and is in good agreement with the one predicted by the detonation polar, 45° . The method of characteristics (MoC) is an exact method for steady supersonic flow when the number of characteristics is sufficient.

In the previous paper of authors,³⁹ the numerical methods of AMROC are compared with those using the MoC.¹⁰ The AMROC solutions are in good agreement with the MoC results. Therefore, the above proves the reliability of the code (AMROC) used in this paper.

The numerical detonation simulation results are sensitive to the grid length scale. Two scales of mesh are selected for a mesh resolution and convergence study to ensure the independence of the results with respect to the grid scale. Coarse mesh: minimum mesh size is $6.25 \times 6.25 \mu\text{m}^2$ for level 3 refinement; Fine mesh: minimum mesh

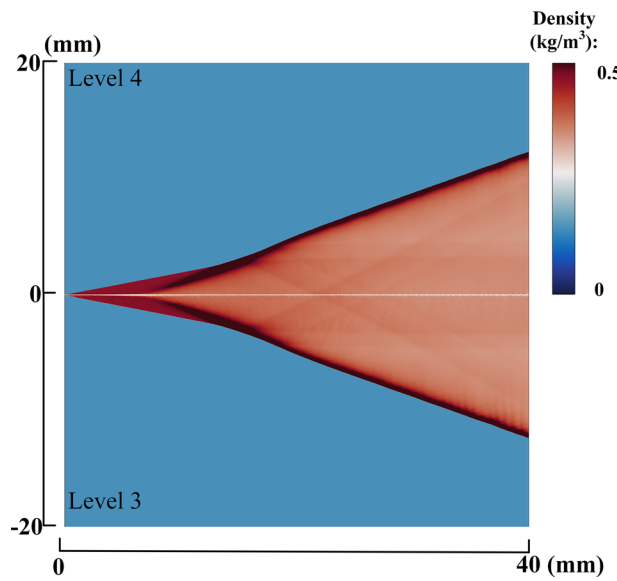


FIG. 3. Density fields with different grid scales in case 2.

size is $3.125 \times 3.125 \mu\text{m}^2$ for level 4 refinement. And, the refinement factor is set as 2 for each level. As shown in Fig. 3, the density flow field of the ODW is basically consistent and difficult to distinguish as well. A quantitative comparison is conducted by plotting the pressure and temperature along three typical lines (i.e., $y = 0, 2$, and 10 mm), as shown in Fig. 4. These lines correspond to different flow regions of the ODW field, including the wedge surface, OSW surface, and steady ODW surface. The curves nearly overlap with trivial differences. Therefore, coarse mesh ($6.25 \times 6.25 \mu\text{m}^2$ for level 3 refinement) is sufficient to capture the main ODW structures. To capture the structure of ODW flow fields in more detail, the fine mesh ($3.125 \times 3.125 \mu\text{m}^2$ for level 4 refinement) is selected in this paper. At present, the grid resolution in most published articles is less than 100 points per half-reaction length,^{21–23} so such a high grid resolution used in this paper

ensures the accuracy and feasibility of the simulation results and leads to reveal the detailed flow field and the evolution of the triple points that have not been paid attention to before during the transition process of OSW–ODW.

IV. RESULTS AND DISCUSSION

A. The formation of smooth oblique detonation

Figure 5 shows the diagram of Mach number and locally enlarged temperature and pressure at $t = 2.5 \mu\text{s}$ when the ODW flow field is established as well as the parameters variation curve along the streamline of case 2. Based on the changes in temperature, pressure, and components on the streamline, first of all, an OSW is generated at the tip of the wedge when inflow enters the flow field. The flow field downstream is not stable, so a weak compression wave (CW) is formed between the OSW and the flow field downstream to balance the pressure in the flow field. A triple point is formed on the shock front and moves downstream. A thin chemical reaction layer is formed on the wedge surface, which shows KH instability near the wedge surface as well as the slip line. However, the chemical reaction is slow at this time, and the flow field is similar to that of unreactive flow.

With the passage of time, the diagram of Mach number, local enlarged pressure, and parameters variation curve along the streamline in the flow field of case 2 at $t = 14.8 \mu\text{s}$ are shown in Fig. 6. The expansion rate of the reaction front becomes faster, the reaction layer becomes thick, the chemical reaction rate accelerates, and the deflagration surface begins to form. With the expansion of the combustion products, the distance between the deflagration surface and the OSW (induction length) decreases, and the intensity of deflagration gets higher, approaching CJ conditions. Moreover, the new triple points are formed and propagate downstream along the wave front, which stabilizes the front of OSW and ODW behind. It indicates that the motion of the triple points can stabilize the uneven internal flow field until a stable ODW is formed.

Figure 7 shows the pressure in the flow field and the motion of triple points at different times after the OSW–ODW transition of case 2. Before the ODW flow field reaches the state of dynamic stability, the unstable motion of shocks coexists with combustion in the flow field. The compression waves in the flow field and the expansion

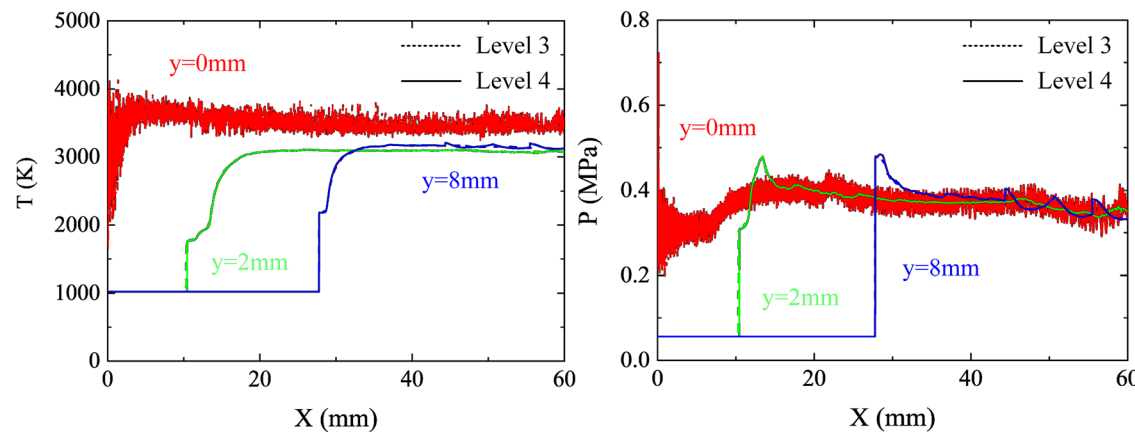


FIG. 4. (a) Temperature and (b) pressure along different lines parallel to the X-axis with different grid scales in case 2.

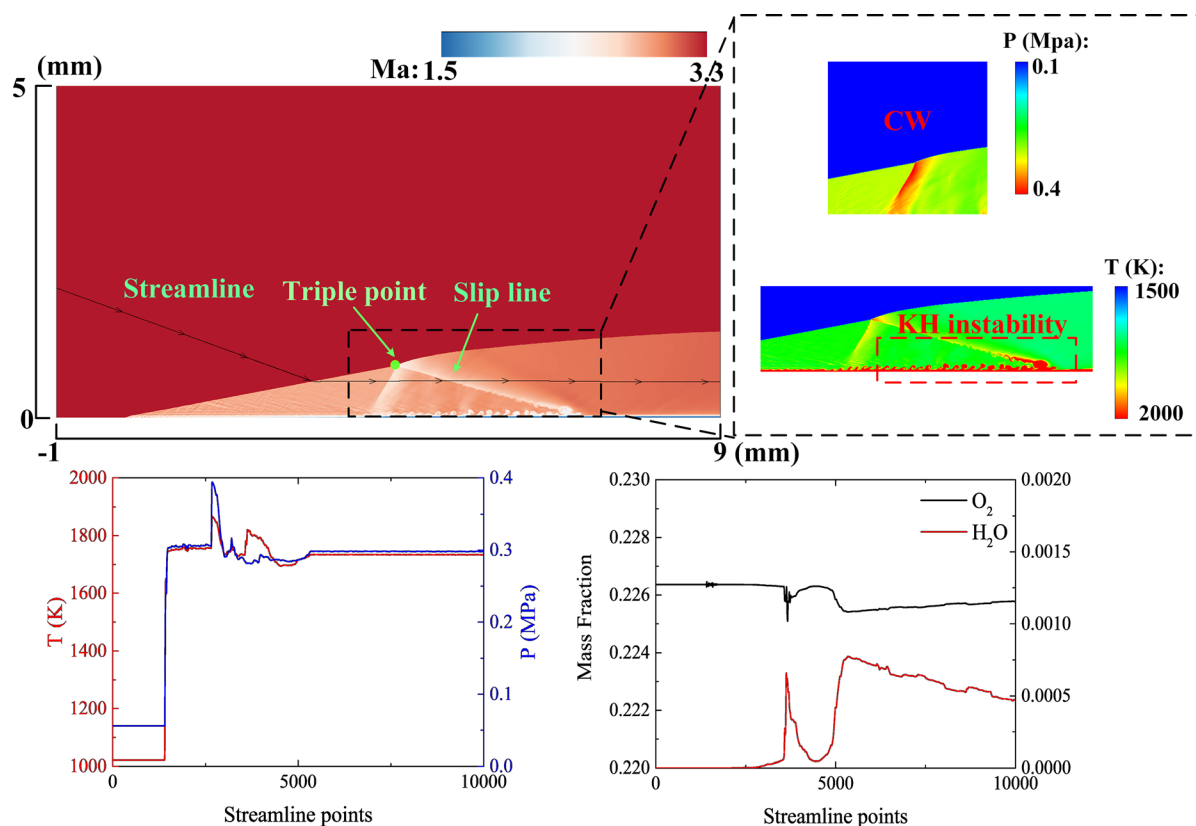


FIG. 5. Diagram of Mach number, local enlarged temperature and pressure at $t = 2.5 \mu\text{s}$, and the parameters variation curve along the streamline of case 2.

waves generated by combustion are able to produce subtle perturbations on the ODW front. These disturbances cause the shock front to create a Y -direction pulsation, or changes in the shock angle, and cause the transverse waves to occur as well. However, because the chemical reaction is not intense at this time, the disturbance intensity is weak, and the fluctuation of the shock angle is small as well, so the number of transverse waves is dense, and the intensity is weak, which shows that the ODW front is unstable, and the frequency of pressure fluctuation is high, and the amplitude is small. However, as the chemical reaction becomes more and more intense, the expansion of combustion products can significantly affect the shape of the ODW front. The formation of the triple point is significantly stronger at this time. The sudden rise in pressure near the triple point results that the pressure is higher than the theoretical pressure of the stable overdriven ODW, which means that the energy generated by the reaction zone is not able to maintain the pressure rise in the triple point. Therefore, the shock angle is reduced until it encounters the next triple point, which is manifested as a cyclic pulsation of pressure on the detonation front, and the frequency of pressure fluctuation between the triple points decreases, but the amplitude increases, as shown by the pressure curve of detonation front in Fig. 7. With the passage of time, the chemical reaction and the position of the shocks reach the state of dynamic stability. There is no disturbance in the flow field and other unstable factors. The transverse waves and triple points move along the ODW front downstream, and the ODW front eventually becomes smooth

and stable. This is the essence of the triple points to stabilizing the detonation front.

The parameters of a line parallel to the Y -axis and crossing the stable ODW front (e.g., $x = 30$ in Fig. 7) are extracted, as shown in Fig. 8. The dashed line represents the CJ temperature and pressure calculated by Cantera³⁷ under the conditions of inflow in this paper, which are 3012 K and 0.25 MPa, respectively. The induction length is 0.59314 mm. Compared with the CJ value, the temperature in the flow field is similar, the pressure is slightly higher, and the induction length is slightly lower, which is 0.28 mm.

Figure 9 shows the smooth transition structure and a more detailed triple point structure. The main structure of transition is two compression waves accompanied by a chemical reaction, and the front of the waves is unstable. A more detailed schematic structure is shown in Fig. 11. Similarly, the detailed structure of the triple points is also enlarged. It can be found that there is a Mach stem between the transverse wave, OSW, and ODW, and a shock wave is used to balance the pressure of the flow field near the triple points; therefore, the final structure of the triple point is y-shaped.

Pressure traces along different streamline lines through the transition structure of the flow field in Fig. 9 are shown in Fig. 10. The compression strength of the fluid passing through OSW on streamline 1 is the same as that on streamline 2, but the burning strength of the deflagration surface on streamline 1 is lower than that on streamline 2. Pressure peaks on streamlines 3 and 4 are almost the same and higher

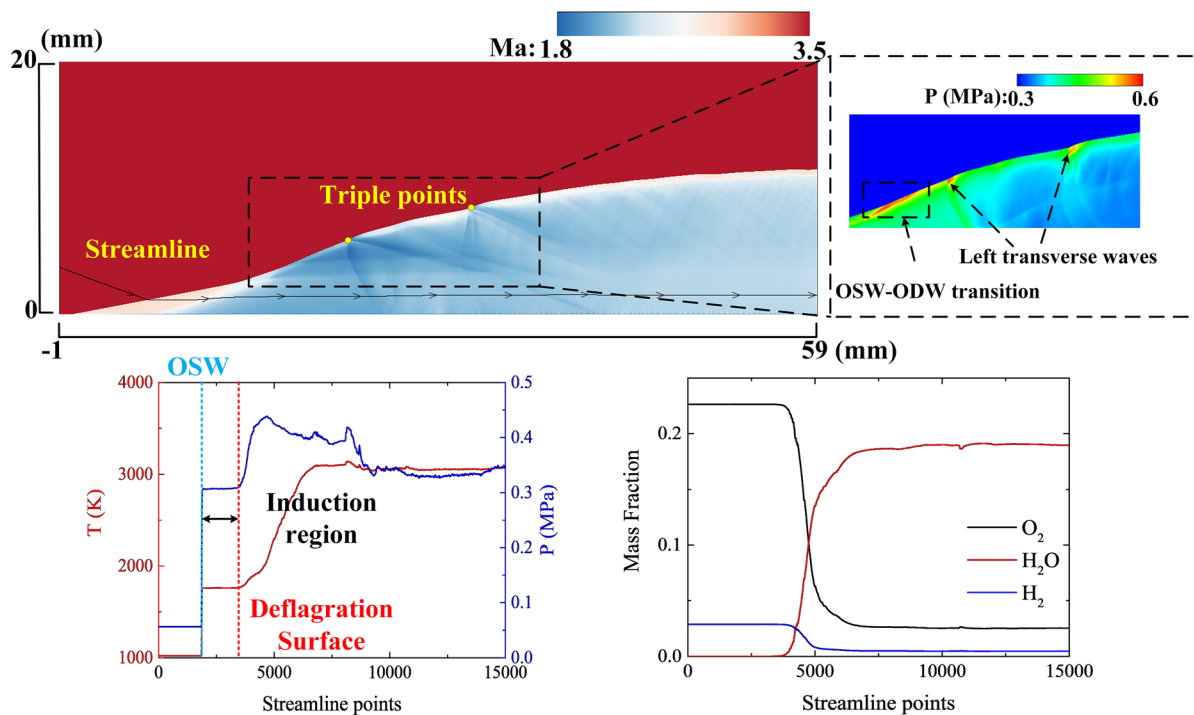


FIG. 6. Diagram of Mach number, local enlarged pressure at $t = 14.8 \mu\text{s}$, and the parameters variation curve along the streamline of case 2.

than on streamlines 1 and 2, indicating that the OSW on streamlines 3 and 4 has been transformed into an ODW. The differences are that the detonation front on streamline 4 is an overdriven detonation, and the inflow pressure is compressed to a value higher than stable ODW, as compared with Fig. 8. The first compression of inflow on streamline 3 is almost the same as that of stable ODW, but after that, the inflow does not expand and decompress but continues to be compressed until it reaches the intensity of overdriven detonation wave, which is called transitional detonation in this paper.

Based on the analysis above, the detailed schematic structure at the smooth transition position of OSW–ODW is extracted, as shown in Fig. 11. There is a curved transitional detonation wave between the OSW and ODW, and the three waves are separated by two compression shock waves. The temperature and density of the flow field after the three waves are discontinuous, while the velocity and pressure are continuous, resulting in two slip lines. The two transitional compression shock waves and the reaction front generate reflected shock waves at the slip line. The position with higher heat release rate (HRR) represents the position of the reaction front, and a discontinuity occurs at the position of the slip lines. When the OSW–ODW transition occurs, the pressure is the highest, and the overdriven detonation is generated and then decays to a CJ detonation.

The variation of parameters and structures in the process of the initiation of the ODW flow field is analyzed in this section. More importantly, the detailed triple point structure and schematic diagram of the OSW–ODW transition structure are extracted. Similar to the DDT process, the transition process and structure are analyzed in detail, which provides a certain reference for the prediction of ODW flow field structure.

B. The formation of abrupt oblique detonation

The formation of ODW and the smooth transition structure of OSW–ODW are analyzed in detail in Sec. IV A. In this section, the inflow temperature, pressure, and Mach number in case 2 were changed to 765 K, 33.5 kPa, and 3.94, respectively, to form an abrupt-type ODW and analyze its transition structure. First, the initial OSW flow field and the reaction layer thickening process are the same as the smooth-type ODW in Sec. IV A. However, due to the decrease of inflow energy, the OSW–ODW structure changes. The transitional detonation, overdriven detonation, and triple point of the abrupt-type ODW have changed relative to the smooth-type ODW in Sec. IV A, as indicated in Fig. 12. The HRR represents the location of the detonation reaction zone. The initiation of ODW is similar to the DDT transition process of normal detonation. When the reaction zone is “catching” the OSW, the distance between OSW and expansion waves with high HRR decreases and eventually couples into an unstable overdriven detonation, which affects the stability of the detonation front. As the heat release is insufficient to support the intensity of the overdriven detonation and the overdriven detonation decays to a CJ detonation, the instability caused by the heat release diminishes and eventually disappears and brings a stable detonation front. Therefore, the instability of the detonation front is due to the expansion waves perturbation caused by the heat released during the initiation process of ODW. However, when the overdriven detonation decays to a CJ detonation, the perturbation disappears, which leads to the stabilization of the detonation front.

Similar to Fig. 10, streamlines at four typical positions in the OSW–ODW transition structure were taken and the pressure on the

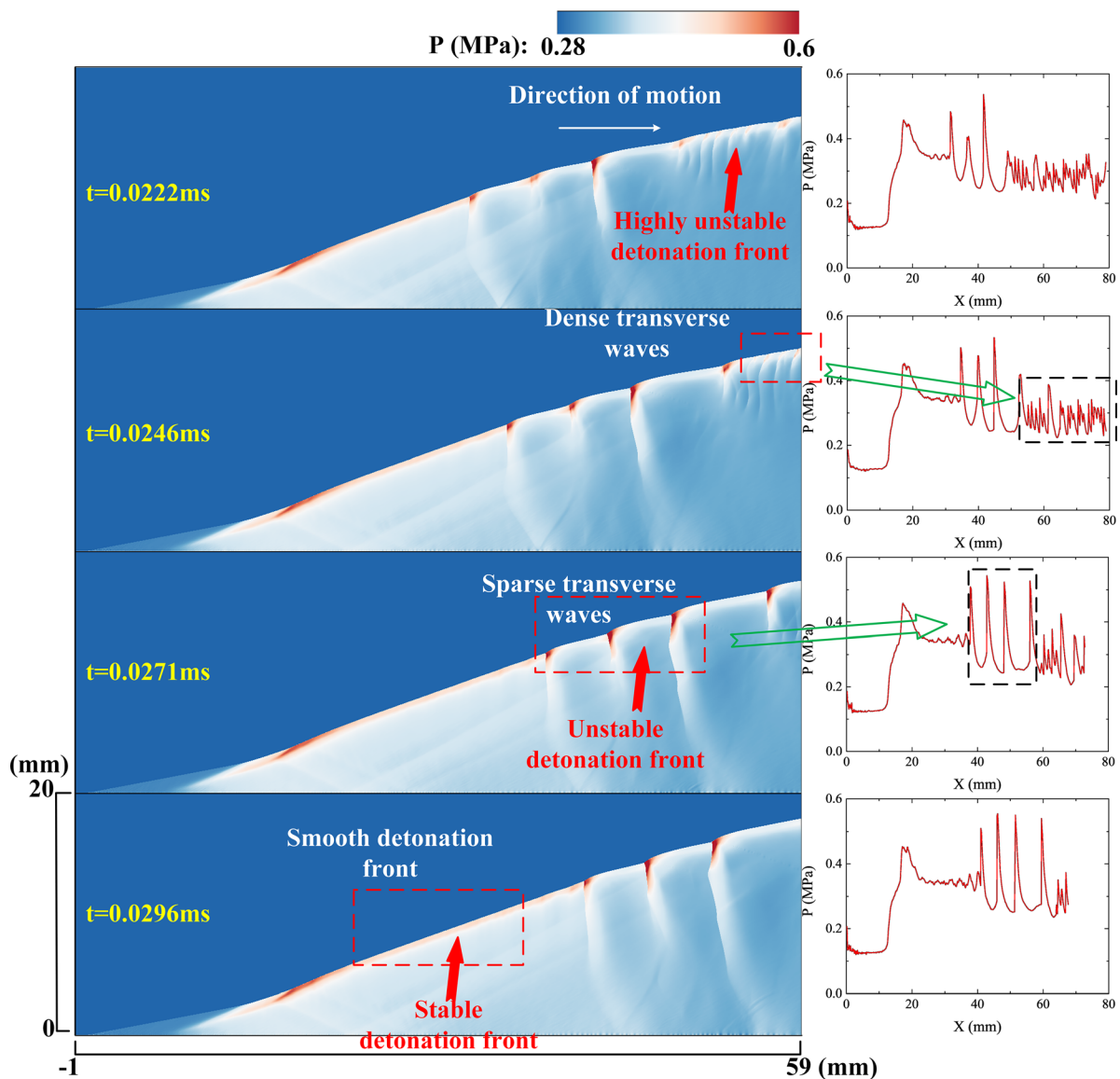
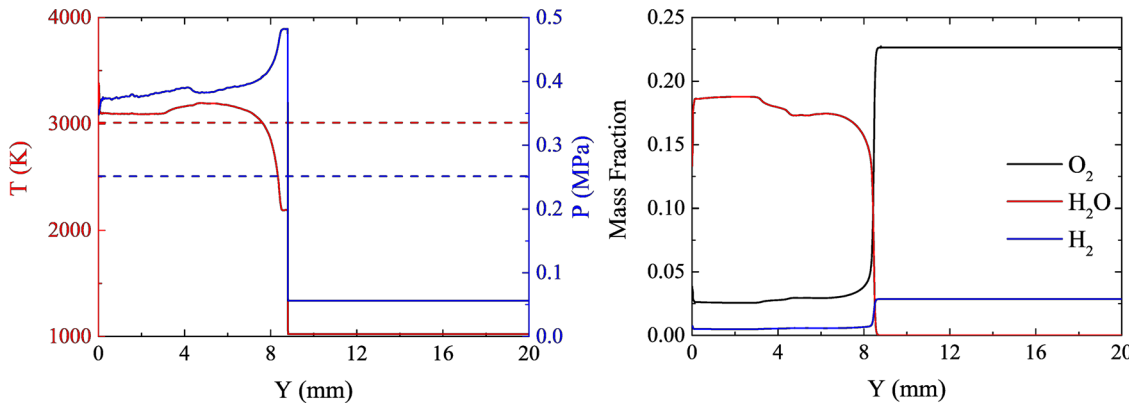


FIG. 7. Diagram of pressure in the flow field after OSW–ODW transition at different times of case 2.

streamlines was compared, as shown in Fig. 13. The pressure variation on the four streamlines is the same as that on the streamlines of smooth-type ODW in Fig. 10. The only difference is that in the smooth-type ODW, the triple point is formed by OSW, transitional detonation, and weak CW. However, now, the triple point is formed by OSW, ODW, and overdriven detonation in the abrupt-type ODW, as shown in Fig. 14. The angle and intensity of OSW change when the inflow Mach number is reduced. The energy of inflow is lower after being compressed by OSW, so the induction time is longer, resulting in an increase in the formation time of ODW. In the process of oblique detonation initiation, the transitional detonation and overdriven detonation are formed before the triple point. As can be seen from the

pressure distribution along streamlines in Fig. 13, the front pressure of the transitional detonation and overdriven detonation is different from the stable oblique detonation on streamline 4. This means that the detonation front is not stable. The upward expansion velocity of combustion products is so fast that it affects the flow parallel to the wedge, which can be seen from the deflection angle of the streamline lines. Finally, the position of the triple point is stable on the ODW, forming the shape of an abrupt-type ODW. In this process, because the intensity of the OSW and ODW differs greatly, there is no transition wave between OSW and ODW, resulting in the formation of Mach stem at the triple point to form a γ -shaped structure, similar to the triple points downstream of the smooth-type ODW in Fig. 9.

FIG. 8. Temperature, pressure, and components along $x = 30$ mm in Fig. 7.

C. A method of transition point prediction for oblique detonations

In the process of the initiation of the ODW flow field, the OSW compresses the pressure and temperature of the reactants, and then, the rapid chemical reaction begins at some point near the wall. In the process of rapid expansion of combustion products, the angle between the deflagration surface and the wall is greater than that between the OSW and the wall. In the direction normal to the OSW, the deflagration flame gradually approaches the OSW, and then, the ODW is generated. Based on Secs. IV A and IV B, a theoretical model for predicting the position of the triple point is proposed in this section, which is of certain reference for predicting the structure of the oblique detonation flow field. The following is a detailed analysis of this process.

Figure 15 is a schematic diagram of the ODW flow field. First, whether the transition is smooth or abrupt, this model predicts the triple point that connects the transitional detonation to the ODW. The turning angle of the first OSW can be obtained by Eq. (11) in gas dynamics,

$$\frac{\tan(\beta_1 + \theta)}{\tan \beta_1} = \frac{(\gamma + 1)M_1^2 \sin^2(\beta_1 + \theta)}{(\gamma - 1)M_1^2 \sin^2(\beta_1 + \theta) + 2}. \quad (11)$$

In the ODW flow field, the angle of OSW and the inflow Mach number basically satisfy Eq. (11), indicating that the first OSW has nothing to do with whether the inflow is a reactant. Thus, β_1 is determined when the inflow Mach number is constant. Based on Fig. 15,

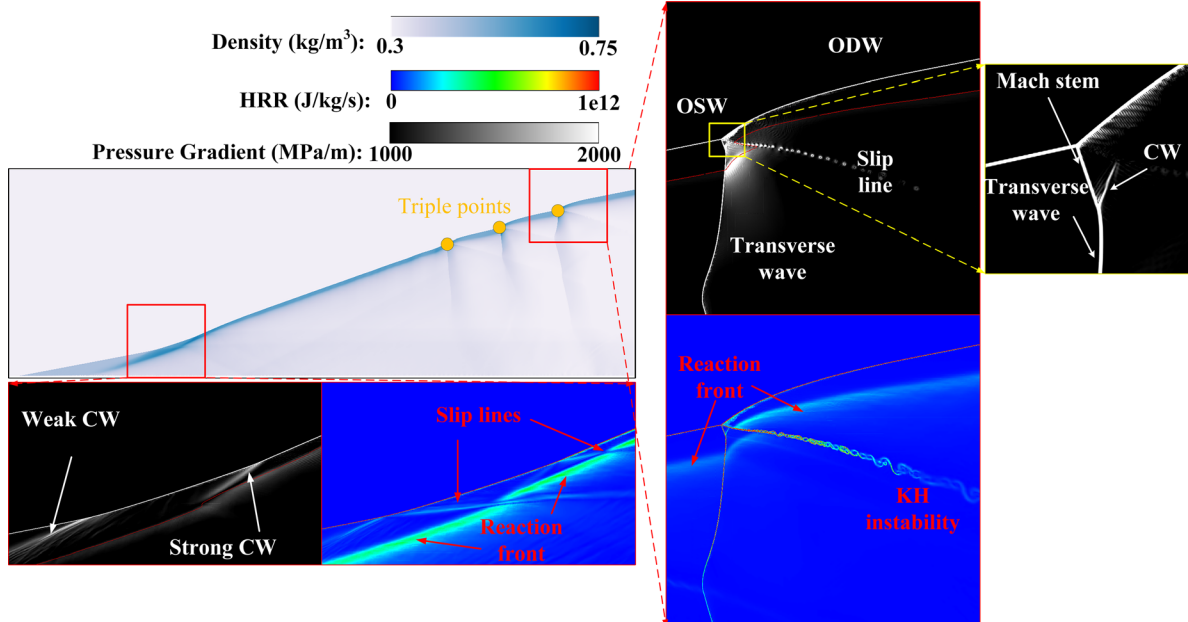


FIG. 9. Enlarged diagram of smooth transition structure and triple points structure.

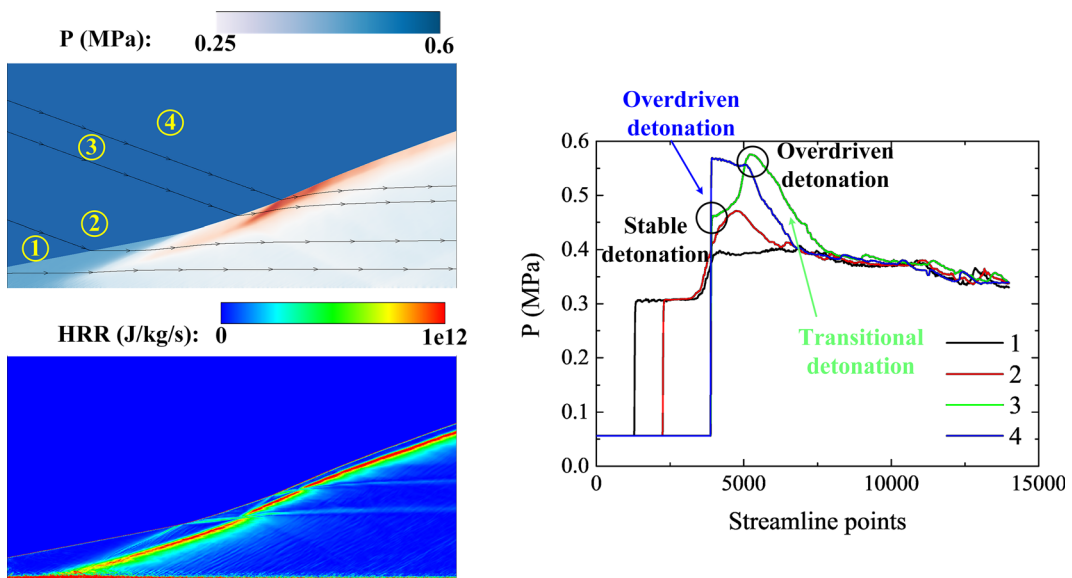


FIG. 10. Pressure on different streamline lines through smooth transition structure of the flow field in Fig. 10.

$$\tan \beta_1 = \frac{y}{x} = \frac{V_3 t}{\delta + V_2 t}, \quad \tan \beta_2 = \frac{y}{x - \delta} = \frac{V_3 t}{V_2 t}. \quad (12)$$

Due to the slow combustion rate of deflagration surface, the parameters such as pressure, temperature, and velocity change slowly. \$V_2\$ is considered a constant value, which can be directly calculated by Eq. (11). The \$\gamma\$ before and after OSW and ODW is assumed to be a constant, respectively. \$V_3\$ is the expansion velocity of combustion products, that is, the deflagration velocity. As the reaction layer thickens from the wedge, the flame surface remains flat. It can be considered that the maximum deflagration velocity is reached when the products begin to expand. According to CJ theory, the maximum deflagration velocity is about 1/2 of CJ detonation velocity. After passing

the first OSW, the movement direction of inflow is parallel to the wall, and the reaction layer becomes thick at a certain point that is defined as the deflagration surface starting point \$\delta\$. Following Refs. 36 and 40, a theoretical approach based on constant volume combustion (CVC) theory is used to estimate \$\delta\$ with post-oblique-shock conditions. It assumes a flow structure where, near the wedge, the mixture is completely burned, and pressure build-up and the formation of pressure waves are weak. The initiation is assumed to be kinetically controlled. In this work, all calculations are performed using the CHEMKIN. First, the post-oblique-shock specie densities and temperature are used to simulate CVC to obtain the reaction time required to attain a mixture temperature with a 10% increase from its post-shock value. The initiation length \$\delta\$ is then calculated by multiplying the time with the post-oblique-shock particle velocity. Despite a simple formulation, this analysis provides a predictive approach for the general structure of oblique detonations.^{36,40} Under the assumption above, the position of the triple point and the angle of the deflagration surface can be simply predicted.

Based on the above prediction model, the pressure gradient diagrams of case 1, case 2, case 3, and the abrupt case are shown in Fig. 16. The yellow dots represent the position of the triple point. The red line represents half of the \$\text{H}_2\text{O}\$ mass fraction after complete reaction in the flow field and the position of the rapid reaction, which is defined as the deflagration surface or reaction front in this paper. Figure 16 proves the theoretical analysis of the interaction of the deflagration surface and ODW, and structure changes in the formation process of ODW in Secs. IV A and IV B.

Table II summarizes the relevant parameters required by the prediction model above, and the comparison between the prediction and the simulation results in different cases, in which the parameters with upper quotes are the theoretically predicted values, otherwise the numerical simulation values. The theoretical prediction error of the triple point position is about a few millimeters, which is small enough

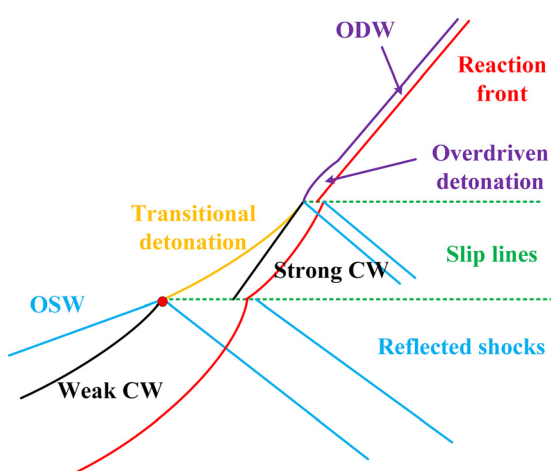


FIG. 11. Schematic of detailed structure at the smooth transition position of OSW-DOW.

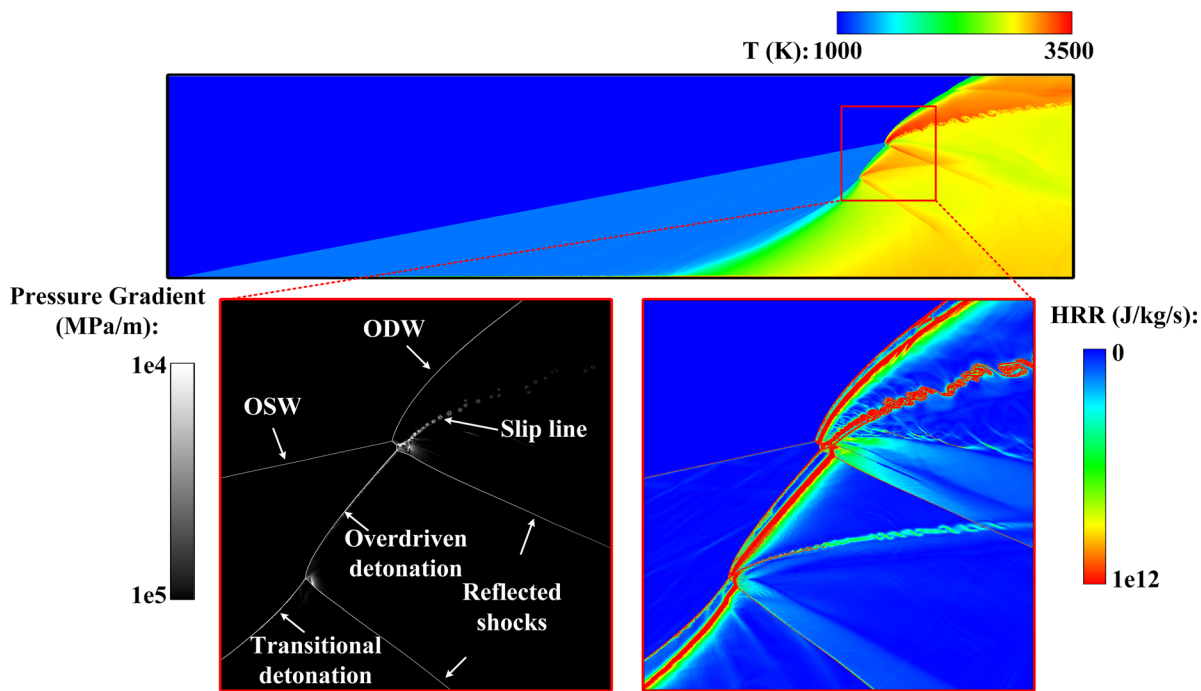


FIG. 12. Enlarged diagram of the abrupt transition structure.

to be acceptable. It is worth mentioning that in the whole prediction model, all parameters are derived theoretically, and the basic configuration of the ODW flow field can be roughly described theoretically under given flow conditions.

This section proposes a simple theoretical prediction model that predicts the triple point. The prediction model is analyzed and verified in detail and compared with the flow field obtained by numerical simulation. The results show that, based on the assumptions in this paper, the error of the theoretical prediction model for the position of the

triple point is relatively acceptable for such a simplified model. However, in order to predict the flow field of ODW more accurately, improvement is necessary, which is also the main work in the future.

V. CONCLUSIONS

In this study, two-dimensional simulations are carried out in order to investigate the formation and evolution of the oblique detonation induced by wedges at different angles and inflow conditions, a detailed model of the transition structure of OSW–ODW is analyzed,

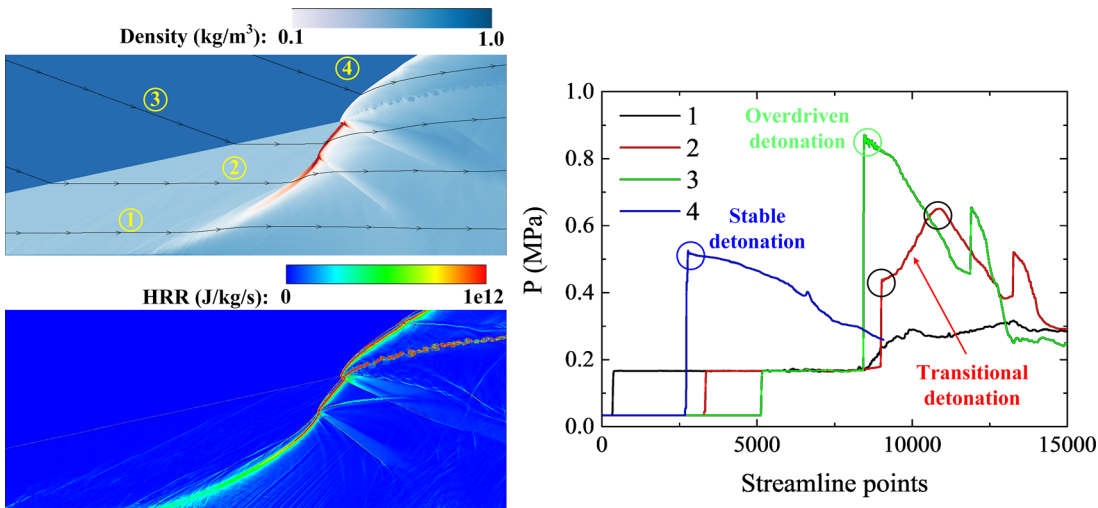


FIG. 13. Pressure and HRR on different streamline lines through abrupt transition structure.

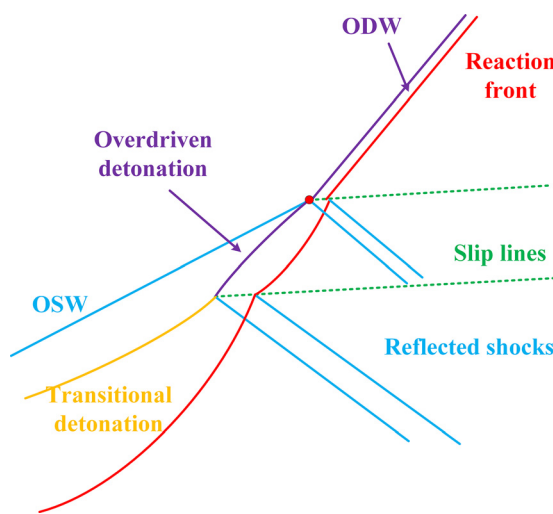


FIG. 14. Schematic of detailed structure at the abrupt transition position of OSW–ODW.

and a theoretical prediction model that predicts the triple point is proposed.

The first process of OSW–ODW is similar to the oblique shock flow field without reactive inflow, whether the OSW–ODW transition pattern is smooth or abrupt. During the short chemical reaction induction time, OSW is generated at the tip of wedge and followed by a curved shock. A weak compression wave is formed between the OSW and curved shock to balance the pressure in the flow field. Therefore, a triple point on the wavefront and thin chemical reaction layer on the wedge surface are formed when the wedge-induced

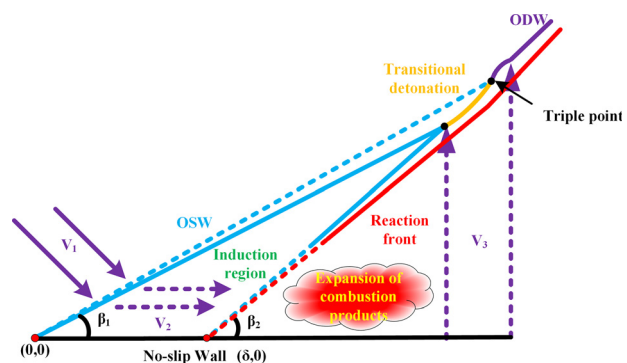


FIG. 15. Schematic diagram of the ODW flow field.

shock preheating premixed inflow, in which KH instability is obviously shown near the wedge surface as well as slip line. With the passage of time, the reaction layer thickens due to the fast expansion rate of the reaction front, and the deflagration surface begins to form.

The second process is similar to the process of DDT. The distance between the deflagration surface and the OSW decreases, and the intensity of deflagration gets higher, approaching CJ conditions, and eventually couples into an unstable overdriven detonation, which affects the stability of the detonation front. As the heat release is insufficient to support the intensity of the overdriven detonation and the overdriven detonation decays to a CJ detonation, the instability caused by the heat release diminishes and eventually disappears and brings a stable detonation front. Moreover, due to the relative position of transitional detonation, overdriven detonation, and the triple point of the abrupt-type ODW have changed compared to the smooth-type ODW,

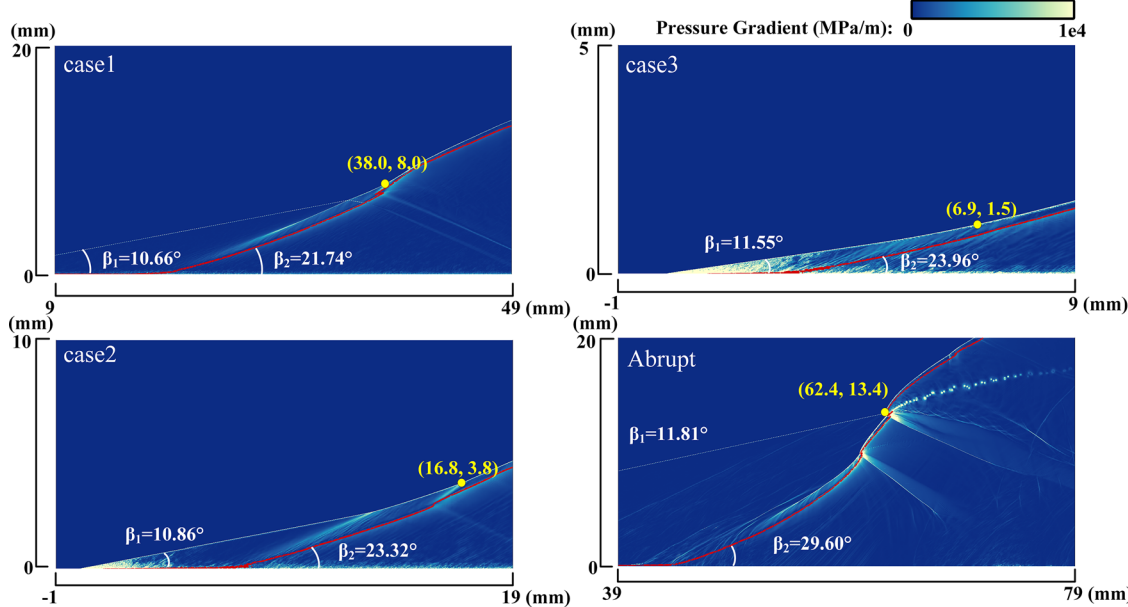


FIG. 16. Verification of the prediction model of the ODW flow field.

TABLE II. Comparison of parameters of the theoretical prediction model in different ODW flow fields.

	θ (°)	δ (mm)	M ₂	V ₂ (m/s)	β_1 (°)	β_2 (°)	β_2' (°)	(x, y) (mm, mm)	(x', y') (mm, mm)
Case 1	15	18.4	3.22	2983	10.66	21.74	17.18	(38.0, 8.0)	(53.2, 10.0)
Case 2	20	7.0	2.85	2865	10.86	23.32	17.61	(16.8, 3.8)	(24.5, 4.7)
Case 3	25	2.9	2.47	2701	11.55	23.96	18.25	(6.9, 1.5)	(15.3, 3.1)
Abrupt	20	43.4	2.54	1942	11.81	29.60	25.70	(62.4, 13.4)	(68.1, 13.4)

the detailed structure of smooth and abrupt ODW is compared and analyzed, and schematic diagrams are presented.

Finally, a simple theoretical method to predict the triple point is proposed. The prediction model is analyzed and verified based on the numerical simulation results in this paper. The results show that, based on the assumptions in this paper, the error of the theoretical prediction model for the position of the triple point is relatively acceptable. However, more validation and accurate revisions for this model are expected in the future.

ACKNOWLEDGMENTS

This work is supported by the National Natural Science Foundation of China (Grant Nos. 51876182, 51406171, and 11972331) and Fundamental Research Funds for the Central Universities of China (Grant No. 20720180058).

AUTHOR DECLARATIONS

Conflict of Interest

The authors have no conflicts to disclose.

Author Contributions

Zhenye Luan: Validation (equal); Writing – original draft (equal); Writing – review and editing (equal). **Yue Huang:** Conceptualization (equal); Funding acquisition (equal); Resources (equal); Writing – review and editing (equal). **Ralf Deiterding:** Software (equal); Writing – original draft (equal). **Yancheng You:** Conceptualization (equal); Supervision (equal).

DATA AVAILABILITY

The data that support the findings of this study are available from the corresponding author upon reasonable request.

REFERENCES

- ¹R. A. Gross, "Oblique detonation waves," *AIAA J.* **1**(5), 1225–1227 (1963).
- ²D. T. Pratt, J. W. Humphrey, and D. E. Glenn, "Morphology of standing oblique detonation waves," *J. Propul. Power* **7**(5), 837–845 (1991).
- ³J. M. Powers, "Oblique detonations: Theory and propulsion applications," in *Combustion in High-Speed Flows*, edited by J. Buckmaster, T. L. Jackson, and A. Kumar (Kluwer Academic, Norwell, MA, 1994), pp. 345–371.
- ⁴C. I. Morris, M. R. Kamel, and R. K. Hanson, "Shock-induced combustion in high-speed wedge flows," *Symp. (Int.) Combust.* **27**(2), 2157–2164 (1998).
- ⁵D. S. Stewart and A. R. Kasimov, "State of detonation stability theory and its application to propulsion," *J. Propul. Power* **22**(6), 1230–1244 (2006).
- ⁶J. Urzay, "Supersonic combustion in air-breathing propulsion systems for hypersonic flight," *Annu. Rev. Fluid Mech.* **50**(1), 593–627 (2018).
- ⁷J. M. Powers and K. A. Gonthier, "Reaction zone structure for strong, weak overdriven, and weak underdriven oblique detonations," *Phys. Fluids* **4**(9), 2082–2089 (1992).
- ⁸J. M. Powers and D. S. Stewart, "Approximate solutions for oblique detonations in the hypersonic limit," *AIAA J.* **30**(3), 726–736 (1992).
- ⁹G. Emanuel and D. Tuckness, "Steady, oblique, detonation waves," *Shock Waves* **13**(6), 445–451 (2004).
- ¹⁰J. Verreault, A. J. Higgins, and R. A. Stowe, "Formation and structure of steady oblique and conical detonation waves," *AIAA J.* **50**(8), 1766–1772 (2012).
- ¹¹D. Martínez-Ruiz, C. Huete, A. L. Sánchez, and F. A. Williams, "Theory of weakly exothermic oblique detonations," *AIAA J.* **58**(1), 236–242 (2020).
- ¹²D. Martínez-Ruiz, L. Scotzniosky, A. L. Sanchez, and F. A. Williams, "Wedge-induced oblique detonations with small heat release," AIAA Paper No. AIAA 2021-0287, 2021.
- ¹³C. Li, K. Kailasanath, and E. S. Oran, "Detonation structures behind oblique shocks," *Phys. Fluids* **6**(4), 1600–1611 (1994).
- ¹⁴V. V. Vlasenko and V. A. Sabel'nikov, "Numerical simulation of inviscid flows with hydrogen combustion behind shock waves and in detonation waves," *Combust. Explos. Shock Waves* **31**(3), 376–389 (1995).
- ¹⁵L. F. F. Da Silva and B. Deshaies, "Stabilization of an oblique detonation wave by a wedge: A parametric numerical study," *Combust. Flame* **121**(1–2), 152–166 (2000).
- ¹⁶K. Ghorbanian and J. D. Sterling, "Influence of formation processes on oblique detonation wave stabilization," *J. Propul. Power* **12**(3), 509–517 (1996).
- ¹⁷J. P. Sislian, R. Dudebout, J. Schumacher, M. Islam, and T. Redford, "Incomplete mixing and off-design effects on shock-induced combustion ramjet performance," *J. Propul. Power* **16**(1), 41–48 (2000).
- ¹⁸G. Fusina, J. P. Sislian, and B. Parent, "Formation and stability of near Chapman-Jouguet standing oblique detonation waves," *AIAA J.* **43**(7), 1591–1604 (2005).
- ¹⁹Y. Zhang, J. Gong, and T. Wang, "Numerical study on initiation of oblique detonations in hydrogen-air mixtures with various equivalence ratios," *Aerospace Sci. Technol.* **49**, 130–134 (2016).
- ²⁰J. H. S. Lee, *Detonation Phenomenon* (Cambridge University Press, 2008), p. 400.
- ²¹H. Teng, H. D. Ng, P. Yang, and K. Wang, "Near-field relaxation subsequent to the onset of oblique detonations with a two-step kinetic model," *Phys. Fluids* **33**(9), 096106 (2021).
- ²²P. Yang, H. D. Ng, and H. Teng, "Unsteady dynamics of wedge-induced oblique detonations under periodic inflows," *Phys. Fluids* **33**(1), 016107 (2021).
- ²³Y. Zhang, L. Zhou, J. Gong, H. D. Ng, and H. Teng, "Effects of activation energy on the instability of oblique detonation surfaces with a one-step chemistry model," *Phys. Fluids* **30**(10), 106110 (2018).
- ²⁴K. Iwata, S. Nakaya, and M. Tsue, "Numerical investigation of the effects of nonuniform premixing on shock-induced combustion," *AIAA J.* **54**(5), 1682–1692 (2016).
- ²⁵K. Iwata, S. Nakaya, and M. Tsue, "Wedge-stabilized oblique detonation in an inhomogeneous hydrogen-air mixture," *Proc. Combust. Inst.* **36**(2), 2761–2769 (2017).
- ²⁶Y. Fang, Z. Hu, H. Teng, Z. Jiang, and H. D. Ng, "Numerical study of inflow equivalence ratio inhomogeneity on oblique detonation formation in hydrogen-air mixtures," *Aerospace Sci. Technol.* **71**, 256–263 (2017).
- ²⁷C. L. Bachman and G. B. Goodwin, "Ignition criteria and the effect of boundary layers on wedge-stabilized oblique detonation waves," *Combust. Flame* **223**, 271–283 (2021).
- ²⁸J. L. Ziegler, R. Deiterding, J. E. Shepherd, and D. I. Pullin, "An adaptive high-order hybrid scheme for compressive, viscous flows with detailed chemistry," *J. Comput. Phys.* **230**(20), 7598–7630 (2011).

- ²⁹R. Deiterding, "A parallel adaptive method for simulating shock-induced combustion with detailed chemical kinetics in complex domains," *Comput. Struct.* **87**(11–12), 769–783 (2009).
- ³⁰M. J. Berger and J. Oliger, "Adaptive mesh refinement for hyperbolic partial differential equations," *J. Comput. Phys.* **53**(3), 484–512 (1984).
- ³¹E. S. Oran and J. P. Boris, *Numerical Simulation of Reactive Flow*, 2nd ed. (Cambridge University Press, 2001).
- ³²M. P. Martín, E. M. Taylor, M. Wu, and V. G. Weirs, "A bandwidth-optimized WENO scheme for the effective direct numerical simulation of compressible turbulence," *J. Comput. Phys.* **220**(1), 270–289 (2006).
- ³³S. Gottlieb, D. I. Ketcheson, and C.-W. Shu, "High order strong stability preserving time discretizations," *J. Sci. Comput.* **38**(3), 251–289 (2009).
- ³⁴P. Kaps and P. Rentrop, "Generalized Runge-Kutta methods of order four with stepsize control for stiff ordinary differential equations," *Numer. Math.* **33**(1), 55–68 (1979).
- ³⁵C. K. Westbrook, "Chemical kinetics of hydrocarbon oxidation in gaseous detonations," *Combust. Flame* **46**, 191–210 (1982).
- ³⁶T. Wang, Y. Zhang, H. Teng, Z. Jiang, and H. D. Ng, "Numerical study of oblique detonation wave initiation in a stoichiometric hydrogen-air mixture," *Phys. Fluids* **27**(9), 096101 (2015).
- ³⁷D. G. Goodwin, R. L. Speth, H. K. Moffat, and B. W. Weber, "Cantera: An object-oriented software toolkit for chemical kinetics, thermodynamics, and transport processes, Version 2.4.0," (2018); available at <https://www.cantera.org>.
- ³⁸C. Viguier, L. F. F. Da Silva, D. Desbordes, and B. Deshaies, "Onset of oblique detonation waves: Comparison between experimental and numerical results for hydrogen-air mixtures," *Symp. (Int.) Combust.* **26**(2), 3023–3031 (1996).
- ³⁹Y. Huang, Z. Luan, Z. Li, H. Ji, and Y. You, "Study on the flow characteristics in the non-detonation reaction zones of wedge-induced oblique detonation transitions," *Aerosp. Sci. Technol.* **120**, 107282 (2022).
- ⁴⁰H. Teng, H. D. Ng, and Z. Jiang, "Initiation characteristics of wedge-induced oblique detonation waves in a stoichiometric hydrogen-air mixture," *Proc. Combust. Inst.* **36**(2), 2735–2742 (2017).